RESEARCH ARTICLE | MAY 23 2025

Origins of NpO_2^{2+} XAS features: Hydrated compared to isolated NpO_2^{2+}

Paul S. Bagus ; Connie J. Nelin ; Michael Trumm ; Bianca Schacherl ; Tonya Vitova

J. Chem. Phys. 162, 204706 (2025)
https://doi.org/10.1063/5.0263322

The Journal of Chemical Physics ARTICLE pubs.aip.org/aip/jcp

Origins of NpO_2^{2+} XAS features: Hydrated compared to isolated NpO_2^{2+}

Cite as: J. Chem. Phys. 162, 204706 (2025); doi: 10.1063/5.0263322
Submitted: 4 February 2025 • Accepted: 5 May 2025 •
Published Online: 23 May 2025

Paul S. Bagus,[1,a)] Connie J. Nelin,[2] Michael Trumm,[3] Bianca Schacherl,[3] and Tonya Vitova[3]

AFFILIATIONS

[1] Department of Chemistry, University of North Texas, Denton, Texas 76203-5017, USA
[2] Consultant, Austin, Texas 78730, USA
[3] Karlsruhe Institute of Technology (KIT), Institute for Nuclear Waste Disposal (INE), P.O. Box 3640, 76021 Karlsruhe, Germany

[a)] **Author to whom correspondence should be addressed:** bagus@unt.edu

ABSTRACT

The principal concern of this paper is to compare theoretical predictions for $M_5 \rightarrow 5f$ x-ray absorption spectroscopy (XAS) obtained between an isolated linear NpO_2^{2+} model and an embedded NpO_2^{2+} model that takes into account the environment of the solution where XAS measurements are actually conducted. The embedded model is an $NpO_2[H_2O]_5^{2+}$ cluster. Novel methods are used to quantify the role of the hydration both for the molecular orbitals and for the many-body wavefunctions that account for the interaction of the hole in the M_5 shell with the two electrons in the open 5f shell of the excited states. It is found that the hydration has only a very minor effect on the XAS excitation energies and intensities, thus validating the previous work based on the properties of an isolated neptunyl cation.

I. INTRODUCTION

The actinides, denoted X, form actinyls with the composition and charge XO_2^{2+}, for X = U to Am, which have short covalent bonds and are associated with a nominal actinide oxidation state of 6+, while the O anions have the nominal charge 2−. They are linear molecules of the form $[O–X(VI)–O]^{2+}$. The character of the actinide–ligand interaction and the role of the covalent mixing of ligand, primarily O(2p), and actinide 5f orbitals were described, in detail, by Denning.[1] They are most often observed in solution, especially in connection with x-ray absorption spectroscopy (XAS) measurements, which are the principal concern of this paper. In particular, for high resolution near-edge XAS (HR-XANES) measurements,[2] the XAS is taken as a slice of a resonant inelastic x-ray scattering (RIXS) map. Although these measurements are made for hydrated systems, these measurements and related theoretical analyses are commonly discussed in terms of the properties of isolated axtinyls; see, for example, Refs. 3–6. Thus, the departures due to these measurement conditions from the theoretical predictions for an isolated linear actinyl need to be quantified and understood. In this paper, the comparison of the predictions for neptunyl (NpO_2^{2+}) between the isolated molecule and the molecule surrounded by five water molecules, $NpO_2[H_2O]_5^{2+}$, is considered. In particular, we study the properties of the Np $3d_{5/2} \rightarrow 5f$ excitations denoted as $M_5 \rightarrow 5f$; we have found in preliminary studies that the changes between the XAS of isolated and hydrated neptunyl are similar for the Np $3d_{3/2} \rightarrow 5f$, denoted $M_4 \rightarrow 5f$, excitations. The objective is to obtain a definitive answer to the question of the extent that the theoretical predictions obtained for isolated neptunyl molecules can be used to model and interpret measurements made on hydrated molecules. As a part of this study, we will examine the effect of hydration for different distances of the embedding water molecules from the neptunyl molecule. We will also justify the use of a smaller active space to determine the wavefunctions of the excited states of the larger models of hydrated neptunyl than has been used in our earlier studies of the XAS of isolated neptunyl.[7,8] For this purpose, we review the choices of active spaces used in our earlier work and examine these choices in the context of the changes to the XAS when different choices are made.

For the 5f shell orbitals, we include both the spin–orbit splitting into $5f_{5/2}$ and $5f_{7/2}$ and also the ligand field splitting in the linear symmetry of neptunyl into 5fϕ, 5fδ, 5fπ, and 5fσ. Indeed, the ligand field splittings are generally larger than spin–orbit splittings. However, it will also be shown that many of the spin–orbit and ligand field splittings are not resolved in the observed RIXS and XAS spectra and the use of theory is required to properly assign the composition of the observed features. The orbitals and wavefunctions (WFs)

for the initial, unexcited configuration and for the excited, $M_5 \rightarrow 5f$, configuration are fully relativistic, including scalar and spin–orbit effects.[9] Of particular importance is that it is not correct to view the $M_5 \rightarrow 5f$ excited states as one electron excitations from one of the six $3d_{5/2}$ shell orbitals into one of the 13 empty 5f shell orbitals where one of the 5f orbitals is already occupied in the initial state. In this view, the excited state would be represented by a single determinant. Indeed, this simple description is approximately valid in only a small number of cases. In fact, the excited states are properly described as multiplets, combinations of determinants, with appropriate angular momentum values.[10] A multiplet may contain only one state or several states with exactly identical energies; indeed, the degeneracies of a multiplet have an important impact on the intensity of the excitation from the initial state to the states of the multiplet.[8] For these many-electron, many-determinantal excited states, the relative intensity of a transition from the initial to an excited multiplet is determined within the dipole approximation.[11] The dipole relative intensity (I_{rel}) is given by

$$I_{rel} = |\langle \Psi(I)|\mathbf{r}|\Psi(F)\rangle|^2. \quad (1)$$

The additional term in the cube of the transition energy required for absolute transition intensities[11] is not included since this term, which varies only very slowly over the range of energies for the excited states, is essentially constant. The matrix element of Eq. (1) is rigorously computed even though, as discussed in Sec. II B, the orbitals used to describe the wavefunctions of the initial and excited states are different. Thus, while the orbitals for each of the initial and excited configurations form orthonormal sets, the sets are not orthogonal to each other. The different orbital sets are necessary to allow for the relaxation of the valence electrons in the presence of the core hole in the excited configurations.[7] The calculation of these matrix elements involves the calculation of cofactors of the overlap integrals for the different configurations times orbital transition integrals, as described by Löwdin.[12]

The many-electron effects discussed in the preceding paragraph lead to transitions from the initial state multiplet into a large number of dipole allowed excited state multiplets, many of which will be unresolved. In Fig. 1, we show our HR-XANES measurements for the $M_5 \rightarrow 5f$ excitations; the relative excitation energies are chosen for comparison with theoretical calculations, which will be presented later, and the intensity is scaled to have the value 0.98 at its maximum. There are three distinct features in the measurement: The leading peak is rather broad with a Full Width at Half Maximum (FWHM) of ~4 eV; it also has a complex structure including a shoulder at ~1 eV higher excitation than the main peak. There is a second measured XAS peak at E(rel) ≈ 10 eV, a third, low intensity, peak at E(rel) ≈ 16 eV, and finally a very low intensity feature at E(rel) ≈ 21 eV, not shown in Fig. 1. The large FWHM, especially of the first peak, clearly indicates that there are unresolved excitations to excited multiplets that cannot be resolved; this is further supported by the asymmetric shape of the first peak. This very strongly indicates that there are a large number of unresolved excitations, contributing to the observed XAS features. This means that the XAS spectra cannot be described as composed of excited states that are single excitations from a $3d_{5/2}$ orbital into one of the unoccupied 5f orbitals. However, the observed spectrum does not allow us to identify the character and energetic spacing of these states. As we will show, our theoretical analysis, presented in Secs. II and III, does, indeed, allow this identification.

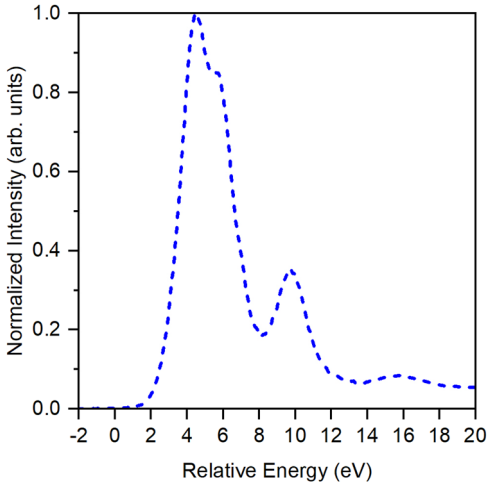

FIG. 1. Measured curve for the $M_5 \rightarrow 5f$ XAS; the measured intensities are scaled so that the maximum has the value of 0.98 in arbitrary units. The choice of zero for the relative is made for comparison with theoretical results to be presented later.

The organization of this paper is as follows. In Sec. II, we describe the methods and methodology for both theory and experiment albeit with a strong focus on the theoretical methods and on the consequences of different treatments of the electronic structure. In Sec. III, the results of the theoretical models for the bare and hydrated clusters are compared with a focus on how the characters of the multiplets change when the environment of NpO_2^{2+} is taken into account. Finally, in Sec. IV, our conclusions are summarized.

II. METHODS AND METHODOLOGY

This section is divided into three subsections. In Sec. II A, we briefly describe the RIXS measurements and the procedure for extracting "measured" XAS spectra from them. In Sec. II B, an overview of the theoretical models for the model systems and of the calculation of the orbitals and WFs is provided. We begin this subsection with a brief comparison of the theoretical results obtained with one of our models with the measured XAS spectra. The intent of this comparison is to show that our theoretical model and methods contain the physical and chemical effects needed to adequately describe the XAS features and demonstrate that our theory can be used to provide fundamental interpretations of origins of the XAS features. In Sec. II C, we describe the methods of analysis of the orbitals and the WFs, especially for the $M_5 \rightarrow 5f$ excited multiplets, and we compare the use of different choices of active spaces for the calculations and their consequences for the XAS spectra.

A. RIXS and XAS measurements

The experimental data were first published in 2017.[2] In brief, Np(VI) was prepared by dissolving $Na_2Np_2O_7$(cr) in 1 mol/l $HClO_4$ solution. The samples were checked for purity by UV–Vis. 135 μl of this solution was placed in a polyether ether ketone (PEEK)

liquid cell and closed with a 10 μm thick Kapton foil and encapsulated by a second containment.[13] The Np M_5 edge (3664 eV) was measured via the Np Mα emission line with a Johann type x-ray emission spectrometer at the INE-Beamline at the KIT Light Source (KIT-LS), Karlsruhe, Germany.[14,15] The beamline setup consisted of a Si(111) double crystal monochromator (DCM) to monochromatize the incident energy and a He-filled box to decrease photon loss by scattering. Five spherically bend Si(220) analyzer crystals at a Bragg angle of 83.42° were aligned in a 1 m Rowland circle to diffract the Np Mα fluorescence onto a Vitus Silicon Drift Detector (SDD). HR-XANES were recorded at the maximum intensity of this emission line. A solid Np^V reference consisting of $K_3[Np^VO_2(CO_3)_2]_{(cr)}$ and $K[Np^VO_2CO_3]_{(cr)}$ was recorded before and after every scan and used for calibration.[16]

B. Overview of models and methods

In order to provide an initial impression of the measured and theoretically predicted spectra, we show in Fig. 2 a comparison between suitably broadened theoretical predictions and HR-XANES measurements for the $M_5 \rightarrow 5f$ XAS. This is done to validate the models and level of theory that we use and to show that they are able to provide us with a meaningful basis for interpreting the XAS spectra. The theory is shown as a solid curve and is labeled as Closed Open Shell Active (OCSA), while the experiment[2] is shown as a dashed curve. The notation OCSA for the level of theory stands for open closed space active which will be explained later. We note that the theory in Fig. 2 is for an isolated NpO_2^{2+} molecule; the changes when the model is hydrated, which are an essential objective of the present work, are considered later. Included in the figure are colored theoretical curves below the full curve, which are transitions to individual final excited multiplets. They are for the broadened excitations to the excited states where only the most intense 20 excitations are shown. These curves are extremely important since they give immediate and direct evidence that many individual excitations underlie the somewhat simpler total XAS curves from either theory or experiment. The theory and the experiment have been rigidly shifted so that the maxima of the most intense excitation of $M_5 \rightarrow 5f$ in theory and experiment have been aligned at the same relative energy, E(rel). Further details of the theoretical results, including the choice of E(rel) = 0 and the broadening of the XAS excitations, are given later in this paper; here, the intent is to provide an initial view of the complexity of the XAS spectra and of the extent of agreement between theory and measurement.

As noted in the Introduction, there are three distinct features in the measurement: The leading peak is rather broad with a Full Width at Half Maximum (FWHM) of ~4 eV; it also has a complex structure including a shoulder at ~1 eV higher excitation than the main peak, which is not present in the theoretical leading peak. The theoretical curve also has a broadened shoulder to lower excitation energies, which is not present in the measured XAS, solid curve. Both of these limitations can be understood to have a common origin in terms of limitations of the theory for the underlying individual excitations as shown by the colored curves for excitations to individual excited multiplets. In the first feature, there are a very large number of underlying contributions from the individual excited multiplets with the largest intensities where the total intensity (black solid curve) is the sum over the intensities to all final states. The large number of colored curves shown in Fig. 2 under the

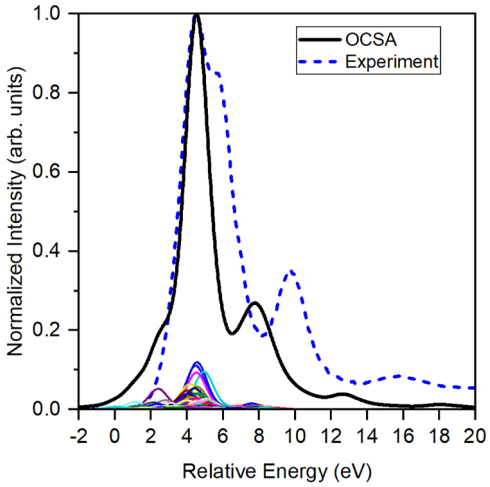

FIG. 2. Comparison of the measured (blue dashed curve) and theoretical (black solid curve) results, for the $M_5 \rightarrow 5f$ XAS. The theoretical intensities are rigidly scaled and rigidly shifted so that the maxima of the theoretical and measured intensities have the same intensity and relative energy; see the text for further details.

first peak all have relatively low intensity, and there is no single large excitation that dominates for this peak. Furthermore, the curves that are shown do not sum to the total intensity, which requires contributions from excitations to other, still less intense, excited $M_5 \rightarrow 5f$ multiplets. One of the limitations of Hartree–Fock theory, and by extension, Dirac–Fock theory, is that the multiplet splittings of different angular momentum couplings of open shell electrons are not given exactly but may have errors of ~1.0 eV; see, for example, Refs. 17 and 18. If one were to shift the individual multiplets shown under the first XAS peak to a higher energy by this uncertainty in E(rel) of ~1 eV, this could remove the low excitation energy shoulder and introduce the higher energy shoulder. This shift could be accomplished by using more accurate wavefunction calculations than those described below; however, this would require significantly more complex and time consuming wavefunction calculations than the limited Dirac–Fock configuration interaction than we have used. Since our objective is not to exactly reproduce the measured XAS but explain the electronic structure that leads to the complex measured spectra shown in Fig. 1, we have not tried to exactly reproduce the observed spectra.

There is a second measured XAS peak at E(rel) ≈ 10 eV, a third, low intensity, peak at E(rel) ≈ 16 eV, and finally a very low intensity feature at E(rel) ≈ 21 eV, not shown in Fig. 2. As for the first, most intense XAS feature, the individual contributions shown in Fig. 2 do not account for the intensity of these other XAS features, which must come from the small contributions from excitations with very small intensity. The overall agreement between the level of theory, denoted as OCSA, and the measured XAS is reasonably good. Although the theoretical values for E(rel) are smaller than the measured E(rel) for these higher excitation energy features by ~2 eV, all the features observed in the measured spectra are in the theoretical predicted spectra. The second peak is predicted at E(rel) ≈ 8 eV compared to the measured E(rel) ≈ 10 eV, and its relative intensity appears to be

somewhat smaller than measured. The third and fourth predicted features are at E(rel) ≈ 13 and 18 eV compared to the measured features at E(rel) ≈ 16 and ≈21 eV. Furthermore, the underlying curves that are shown do not sum to the total intensity, which requires that contributions be included from excitations to other, still less intense, excited $M_5 \rightarrow 5f$ multiplets. This very clearly illustrates that a very large number of unresolved excitations, each with relatively low XAS intensity, contribute to the observed XAS features. In addition, the energetic spread, or range, of the individual theoretical multiplets is narrower than observed. This is not surprising, since the theoretical quantum chemical calculation of very accurate values of multiplet splittings is rather demanding[17] and may require a more extensive treatment of many-body terms than was made for the OCSA calculations shown in Fig. 2. Indeed, if the multiplet splittings were somewhat larger, the first peak would be somewhat broader in better agreement with the measured spectra. In addition, the scaling of the theoretical intensity to match the experimental intensity at the maximum of the first peak would lead, for a broader first theoretical peak, to an increase in the apparent relative intensity of the higher excitation features. Another possible reason for the somewhat smaller theoretical E(rel) compared to experiment is that the theory presented in Fig. 2 is for an isolated NpO_2^{2+} molecule and does not include the effects of the hydration of neptunyl, which is the case for the measurements. Indeed, as we shall show below, the changes induced by using a hydrated, $NpO_2^{2+}[H_2O]_5$, model do act to improve the agreement of theory with experiment.

The models that we use to study the XAS of neptunyl are an isolated linear molecule of $Np(VI)O_2^{2+}$ and a hydrated molecule surrounded by five water molecules, $Np(VI)O_2[H_2O]_5^{2+}$, which are schematically shown in Fig. 3. The embedding with five H_2O molecules to represent the effects of hydration on the neptunyl cation is a suitable choice given our general understanding of the hydration of actinyls in aqueous solution. There are several experimental extended x-ray absorption fine structure (EXAFS) studies, which conclude that $Np(VI)O_2^{2+}$ in solution exists predominantly as a pentaaquoneptunyl complex equatorially coordinated to the neptunyl cation; see, for example Refs. 19 and 20. The base bond distance for R(Np–O) = 1.73 Å as used in our previous studies of NpO_2^{2+}[2,7,8] was used for both the bare and hydrated clusters. For the hydrated cluster, the distances of Np to H_2O and H–O and the H–O–H bond angle were optimized through density functional theory calculations, which used extended basis sets and a B3LYP functional[21,22] to be R(Np–H_2O) = 2.48 Å and R(O–H) = 0.969 Å, and the H–O–H angle is 107.0°. The optimized values for the embedding H_2O molecules are quite close to those of the isolated H_2O molecule,[23,24] where R(O–H) = 0.96 Å and the angle is 104.5°, showing that the interaction of embedding H_2O molecules with neptunyl does not lead to significant changes in their geometry. The distance of Np to the H_2O molecules was varied in the studies of the effect of hydration on the neptunyl properties between 2.48 and 9.44 Å, where the latter distance of NpO_2^{2+} from H_2O was shown to have properties that are essentially equivalent to isolated NpO_2^{2+}. The open shell occupations in the configurations that were used to study the initial, ground state (GS), multiplet and the excited $M_5 \rightarrow 5f$ multiplets were

$$\begin{aligned} &GS - 3d_{5/2}{}^{6}5f^{1}, \\ &M_5 \rightarrow 5f - 3d_{5/2}{}^{5}5f^{2}, \end{aligned} \tag{2}$$

where the $3d_{5/2}$ occupation is included in the GS even though it is fully occupied in this configuration. All shells not shown in Eq. (2) are fully occupied. The shells are shown as pure Np orbitals, even though for the 5f open shell, there is significant covalent, anti-bonding mixing with O orbitals, especially O(2p) orbitals, as will be discussed below. The linear symmetry also leads to a splitting of the $3d_{5/2}$ orbitals into three doubly degenerate shells that are split by only a few milli-electron volts. This small symmetry splitting of the $3d_{5/2}$ orbitals will lead to large numbers of nearly degenerate multiplets for the neptunyl excited states.

The 5f orbitals are considered in more detail. They are split into seven ligand field and spin–orbit split orbitals, which to a good approximation for linear NpO_2^{2+} can be described as

$$5f\phi_{5/2}, 5f\phi_{7/2}, 5f\delta_{3/2}, 5f\delta_{5/2}, 5f\pi_{1/2}, 5f\pi_{3/2}, \text{ and } 5f\sigma_{1/2}. \tag{3}$$

In the $D_{\infty h}{}^{*}$ double group of linear NpO_2^{2+}, only the total orbital angular momentum, ω, indicated by the subscripts in Eq. (3), is a good quantum number. While there can be mixing of orbitals with the same value of ω, this mixing is small. The ordering of the orbitals in Eq. (2) does not follow the order of the Dirac–Hartree–Fock, DHF,[9] orbital energies, ε, except that ε for the lower possible spin–orbit value is always below (lower or more negative) than the ε for the higher value. However, while the spin–orbit splittings of the ε for a given linear symmetry are ~1 eV, the ε splitting between the non-bonding 5fφ and 5fδ and the most strongly anti-bonding 5fσ is ~5–10 eV. While the discussion above applies exactly to the bare NpO_2^{2+}, the additional splittings in the ε introduced for the lower symmetry hydrated cluster, $NpO_2[H_2O]_5^{2+}$, are small and we use the same symmetry notations for the hydrated cluster.

For these two models of NpO_2^{2+} orbitals and total configuration interaction (CI), WFs are determined. The orbitals are variational solutions of the Dirac Hartree–Fock (DHF) equations.[9] Indeed, an important focus of our paper will be to examine the covalent character of these orbitals. The configurations for the DHF calculations are those shown in Eq. (2), where the open shell orbitals are occupied in all possible ways and the orbitals are determined for the average of all these occupations.[25] The total, many-electron, WFs mix determinants with different occupations of the open shell

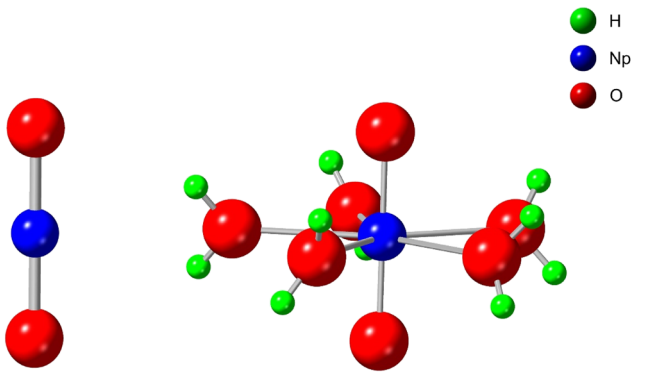

FIG. 3. Schematic representation of the isolated, NpO_2^{2+}, on the left, and the hydrated, $NpO_2[H_2O]_5^{2+}$, on the right.

orbitals; these are described as CI WFs.[17] The CI WFs are needed to obtain WFs that have good total symmetry and thus have exact degeneracies for the different members of a multiplet.[9,17,25] It is stressed that a single determinant is, in general, not sufficient to describe a WF with correct total symmetry; see, for example,c Ref. 18. The CI may also be needed to treat the many-body effects that are needed to correctly describe the WFs and the relative energies of different multiplets. The key parameters for the CI WFs are the active spaces for the choice of orbitals that are used to construct the determinants for the CI WFs and the choices of the occupations of the orbitals in the determinants that form the CI expansion of the WF.[8]

Before we consider the choices of active orbital and configuration spaces, we comment briefly on how the XAS spectra are obtained from the WFs for the initial and excited configurations. In Fig. 4, the transitions from the initial state, or GS, multiplet to the different excited configuration multiplets are shown schematically. This figure shows the transitions as dotted lines from the GS multiplet to three different possible excited state multiplets where the transition energy is simply the energy difference of the WFs. Although only three excited multiplets are shown, there are a much larger number of excited states that may gain intensity. For the GS, one must, in principle, consider a Boltzmann distribution of the occupation of initial states. For NpO_2^{2+} with the initial configuration of Eq. (2), there is only one twofold degenerate multiplet that will be occupied at any reasonable temperature, $(5f\phi_{5/2})^1$, with symmetry Ω = 5/2u; the first excited multiplet is $(5f\delta_{3/2})^1$ at $\Delta E(rel)$ = 0.28 eV. Thus, the choice of the initial state wavefunctions is unique and clearly defined. Meanwhile, there are a large number of dipole allowed excited states[11] with symmetries Ω = 3/2g, 5/2g, and 7/2g. The excitations to multiplets with symmetry Ω = 5/2g are polarized along the molecular axis, while the excitations to Ω = 3/3g and 7/2g are polarized perpendicular to the molecular axis. Closely related considerations apply to the initial and excited state multiplets of the hydrated, $NpO_2[H_2O]_5^{2+}$, cluster.

The dipole transition intensities, see Eq. (1), are taken between the WFs for the initial and final multiplets as shown schematically in Fig. 4 for three representative transitions shown with different colored arrows. The intensities represented are summed over all the states of the final multiplet and averaged over the states of the initial multiplet.[8] In addition, as explained below, the intensities for nearly degenerate states may be grouped together. These directly computed intensities can be viewed as sticks of a certain magnitude (scaled intensities) at the transition energy, which is the difference of the ground and excited state energies as shown by the arrows in Fig. 4. However, in order to compare these theoretical intensities with measured XAS intensities, it is necessary to broaden them to take into account two effects. One arises from the resolution of the measurement, which is represented by a Gaussian broadening with an FWHM of 1.0 eV.[26] The other broadening arises from the lifetime of the M_5 core-excited levels and is represented by a Lorentzian function.[11] The choice of the FWHM for the Lorentzian is 0.5 eV, which is much smaller than the FWHM of 3.6 eV, which is the lifetime of the M_5 level of Np.[27] The choice of a much smaller Lorentzian broadening is because the experimental results that we compare our theoretical results with have a much higher resolution since they are based on RIXS measurements; see Ref. 8 for a justification of the Lorentzian FWHM used. These two broadenings are combined with a Voigt convolution.[28] This leads to the broadened intensities shown as colored curves in Fig. 2. The I_{rel} values shown in Fig. 2 are, as noted above, summed over the I_{rel} of groups of nearly degenerate excited state multiplets, where the multiplets in the group have the same energies within 0.5 eV. This grouping is done to avoid showing many individual excitations to excited multiplets that have virtually identical excitation energies and could not be resolved in XAS measurements; the calculation of the transition intensities is described in Ref. 8, Sec. II C. For the relative energies in Fig. 2, E(rel) = 0 is the lowest energy excited multiplet with the configuration of Eq. (2); if this multiplet is not be dipole allowed, its intensity is, of course, zero. The non-zero intensities into the individual groups are broadened, as explained above, with a Voigt convolution. The individual broadened intensities for the different final, excited state, multiplets are summed to give the total intensity shown as the black solid curve in Fig. 2, while the curves in color represent contributions to the XAS from excitations to groups of almost degenerate excited multiplets. These individual broadened contributions to the XAS are for the most intense groups of multiplets; the large number of these individual groups is clear evidence that the observed XAS cannot be interpreted as an excitation of a single core orbital into a single excited orbital. They are also clear evidence that many individual excitations can and do account for the broad observed XAS features. The broadened intensities in Fig. 2 for the individual contributions, in color, and the total intensity, black curve, are rigidly scaled so that the maximum of the total intensity curve, the black curve, has a value of 0.98. This rigid scaling to a normalized intensity allows us to represent the total XAS as well as its individual contributions in a way that can be directly compared to the XAS measurements.

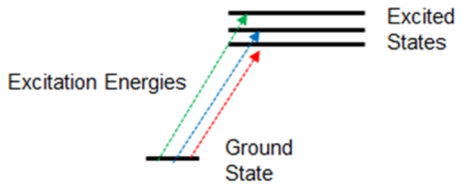

FIG. 4. Schematic representation of excitations from the initial to representative excited multiplets of NpO_2^{2+}.

There are two sets of active spaces that define the WFs. The first is described as Open Shell Active (OSA); these spaces have a direct connection to the open shell configurations in Eq. (2). For the OSA distributions for the initial, GS, state, all possible distributions of one electron over the 14 open shell, dominantly 5f spin orbitals are considered; see Eq. (3). This leads to a 14 determinant CI to determine the GS WFs. The ground state for NpO_2^{2+} is Ω = 5/2u and is almost pure $(5f\phi_{5/2})^1$ with very small mixing with $(5f\delta_{5/2})^1$. For the $M_5 \rightarrow 5f$ excited states, the OSA CI includes all determinants that can be formed with five electrons in the six $3d_{5/2}$ spin orbitals and two electrons in the 14 dominantly 5f open shell spin orbitals; this CI includes 546 determinants. For the states obtained from this CI, only those with the dipole allowed symmetries of Ω = 7/2g, 5/2g, and 3/2g are of interest. The analysis and the sizes of the CIs can be extended directly to the hydrated model of neptunyl, $NpO_2[H_2O]_5^{2+}$. This is because the evidence presented so far and further emphasized in the following material shows that the hydrated neptunyl is simply

a perturbation of the isolated system; this is the main and rather important conclusion of our detailed study.

The Closed Open Shell Active (OCSA) spaces were used only for the excited states. In addition to the 546 determinants for the OSA, determinants with single and double excitations from three closed shell orbitals that had significant contributions of Np 5f character were included in the OCSA CI; see Refs. 7 and 29. These orbitals were bonding between the Np cation and the O anions. In effect, the new determinants can be viewed as involving excitations from bonding into the non-bonding or anti-bonding, dominantly 5f "open" shell orbitals. These additional excitations lead to over 100 000 determinants in the CI calculation for the OCSA WFs. While, as shown below, excitations from closed shell orbitals into the open shell space are needed to correctly describe the energy splittings of the XAS features, the smaller OSA WFs do give a useful description of the main XAS features.

Calculations of the orbitals and WFs were performed with a slightly modified version of the relativistic DIRAC (Direct Iterative Relativistic All-electron) program system.[9,30] The basis sets were fully uncontracted; the exponents for Np were taken from the work of Dyall,[31] and the exponents for O and H were taken from the work of Duijneveldt.[32] The calculations of the XPS intensities were made with programs in the CLIPS program package,[33] where the output of DIRAC has been interfaced to CLIPS (Core Level Ionization Potential System). Programs were written for the Voigt broadening of the XPS.

C. Orbital and wavefunction analysis

We turn now to a brief review of the unique methods that are used to analyze the properties of the orbitals and the total WFs. While it is common to use population analyses to describe the covalent character of orbitals,[34–37] we have developed other techniques to characterize orbitals.[29,38] These techniques are especially useful to describe the covalent character of the molecular orbitals for nominally ionic compounds. One of them is based on the projection of fragment orbitals on the orbitals of bare NpO_2^{2+} or those of embedded $NpO_2[H_2O]_5^{2+}$. The fragment orbitals of interest are the Np 5f orbitals variationally determined as DHF orbitals for the isolated Np^{6+} cation, and the projection on a given compound orbital is a sum of the squares of the overlap of the Np^{6+} orbitals with the compound orbital. The sum over the different 5f orbitals of the cation is needed since different cation Np(5f) orbitals can and do mix in a given compound orbital. The limits of the projection, denoted $N_{Proj}(5f)$, are $0 \le N_{Proj}(5f) \le 1$, where $N_{Proj}(5f) = 0.0$ indicates that the orbital has no 5f character and $N_{Proj}(5f) = 1.0$ indicates that the orbital is a pure Np 5f orbital. There are relatively minor deviations from these ideal values partly because there are minor changes to the Np(5f) radial function depending on the effective charge of the Np and because there is non-zero overlap between the Np(5f) and O(2p) orbitals. However, the trends and the magnitudes of the projections are still very useful to examine the covalent character, especially of the open shell, dominantly Np(5f), orbitals. Another measure of the orbital character is the effective size, or spatial extent, of the orbital, r_{eff}, defined as $r_{eff} = [\langle r^2 \rangle]^{1/2}$, where the origin is taken as the Np center. For a pure Np $5f_{5/2}$ or $5f_{7/2}$ orbital, r_{eff} is 0.8 Å,[39] which is significantly smaller, less than half, of the Np–O distance of ~1.7 Å. Meanwhile, for a pure O(2p) orbital, the r_{eff} will be modestly greater than R(Np–O) since the orbital is centered about the O nucleus. As the covalent character of a neptunium open shell orbital increases, r_{eff} will increase from the value for a pure Np 5f orbital toward the value for a pure O(2p) orbital. A final measure of relative covalent character of the open shell, dominantly Np(5f) orbitals, is given by the DHF orbital energies, ε. A general rule for orbital energies is that bonding character lowers an orbital energy, while anti-bonding character raises an orbital energy. For the application to the ε(5f) of neptunyl, one would expect that the non-bonding 5fφ and 5fδ would have the most strongly bound ε, while the anti-bonding, π and σ orbitals, would have less strongly bound ε. Indeed, the open shell σ symmetry orbital is most anti-bonding and has a significantly larger ε than the open shell π orbital. While these symmetry designations apply rigorously only for NpO_2^{2+}, they remain useful descriptions of the orbital character for $NpO_2[H_2O]_5^{2+}$.

Two properties of the total WFs also provide important measures of the nature of the chemical interaction between the nominally Np^{+6} cation and the nominally O^{-2} anions. The first is the dipole intensity of the transition from the initial, GS, multiplet to an excited configuration multiplet. Clearly, an excited multiplet where there is a large intensity for dipole excitation from the initial state must have significant contributions from configurations that have a dipole allowed $3d_{5/2} \rightarrow 5f$ orbital excitation. This can be quantified through the occupations of orbitals in the many-electron CI WF for the excited state. The occupation of an orbital in a CI WF[8] is a suitably weighted average over the orbital occupations of the individual configurations that contribute to the WF. It will be a value between 0, when the orbital is not occupied in any configuration in the WF, and 2, when the orbital is fully occupied in all configurations in the WF. It is usual to consider the occupations of a shell of electrons rather than the occupations of a degenerate, or nearly degenerate, member of the shell. For the 5f shell, the occupations are summed over the spin–orbit components of the ligand field split orbitals, ϕ, δ, π, and σ. In addition, the occupations of the non-bonding 5fϕ and 5fδ are summed into a single occupation denoted 5f(ϕδ). With these sums, the number of individual occupations considered is 5f(ϕδ), 5f(π), and 5f(σ). There are additional configurations in the OCSA WFs. These configurations involve excitations from the three fully occupied orbitals that, while they have significant bonding Np character, have dominantly O(2p) character. They can be viewed as charge transfer configurations, but we stress that they are best viewed as excitations from bonding to anti-bonding orbitals, which add the necessary many-body effects to correctly describe the energies of the neptunyl $M_5 \rightarrow 5f$ excited. Thus, the occupations of these "closed" shell orbitals show the extent of the closed shell excitations into the open shell space; this occupation is denoted Occ(closed). For these "closed" shell occupations, the departure from full occupation, ΔOcc(closed) = Occ(closed) − 6, is considered. The negative sign for ΔOcc(closed) is chosen so that the sum of the different 5f Occ and ΔOcc(closed) will be 2.0, the nominal 5f occupation in Eq. (2).

Since there are a very large number of excited state multiplets, it is convenient to consider the intensities and occupations for groups of multiplets rather than for individual multiplets. The multiplets are divided into groups in an energy range of ΔE = 0.5 eV; the intensities of the multiplets in the group are summed, and the orbital occupations are averaged over the multiplets in the group.[8] The group intensities and shell occupations for the $M_5 \rightarrow 5f$ excitations for the OCSA CI WFs of NpO_2^{2+} are shown in Fig. 5. The group intensity for group n, $I_G(n)$, is shown in Fig. 5 as a yellow vertical bar with

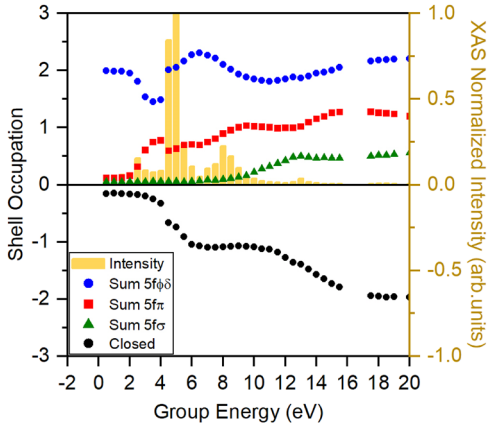

FIG. 5. Group properties for the occupations and intensities of the OCSA $M_5 \rightarrow 5f$ excited multiplets for the isolated NpO_2^{2+} neptunyl WFs; see the text for definitions of the symbols.

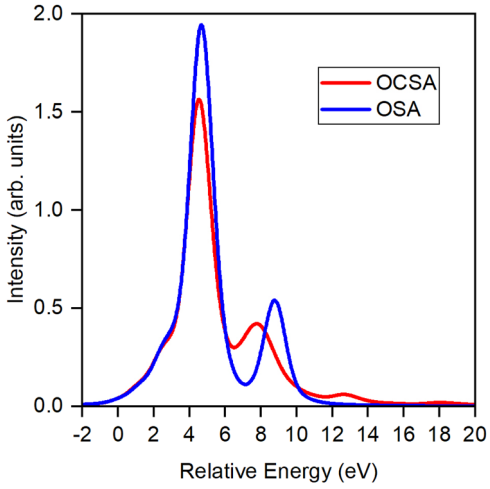

FIG. 6. Comparison of the XAS obtained with two active spaces for isolated NpO_2^{2+}; the smaller OSA space XAS is shown as a blue curve and the larger OCSA space is shown as a red curve; see the text for details.

magnitude given on the right vertical axis. The group intensities are normalized so that the maximum group intensity, at $E_G = 5.5$ eV, is 1.0. This normalization is made so that it is easy to compare intensities for different groups and to compare with the broadened and normalized theoretical spectra. Indeed, the group intensities in Fig. 5 are fully consistent with the broadened XAS theoretical plot in Fig. 2. The group occupations, Occ, for the different 5f sets of orbitals and the ΔOcc for the closed shell orbitals are shown as symbols of different colors and shapes centered about E_G; the symbols are defined in the inset of Fig. 5. We recall that the change in the occupation of the nominally closed shell, dominantly O(2p) orbitals, ΔOcc, which is shown as closed in Fig. 5, shows the importance of many-body effects needed to correctly describe the higher energy excited states in Fig. 2. The values for the shell occupations are given on the left vertical axis. Although the lowest group energy is $E_G = 0$, Fig. 5 starts at $E_G = -2$ to be consistent with the energy scale of the broadened XAS in Fig. 2.

A final consideration in this section is to compare the $M_5 \rightarrow 5f$ XAS predicted using OSA and OCSA WFs. This is done since much of the following discussion and results for the XAS is based on results for the larger hydrated clusters, $NpO_2[H_2O]_5^{2+}$, based on their OSA WFs since the calculations of these WFs is much less demanding than the more accurate OCSA WFs. This approximation is acceptable provided that the differences between the OSA and OCSA XAS are reasonably small. In Fig. 6, the broadened $M_5 \rightarrow 5f$ XAS for isolated NpO_2^{2+} is compared between using OSA WFs, the blue curve, and using OCSA WFs, the red curve.

As distinct from Figs. 1 and 5, the intensities in Fig. 6 are not normalized but are the many-electron intensities from Eq. (1). The intensities are broadened with a Voigt convolution with Gaussian and Lorentzian FWHM as described earlier. The transition energies are given as relative energies, and the curves are aligned so that for the lowest energy excitation, for both OSA and OCSA excitations, E(rel) = 0. There is a similarity for the first, most intense, feature at E(rel) ~ 4 eV between the OSA and OCSA XAS; the maxima are at almost the same E(rel), and the width of the features is almost the same. However, the intensity of the OCSA feature is somewhat lower than that of the OSA feature. This is to be expected since the OCSA WFs include many configurations with excitations from the closed shell space into the open shell space and these configurations are dipole forbidden excitations from the GS. The second feature in the OCSA XAS is at an E(rel) of ~8 eV, which is about an eV less than the OSA E(rel) for this feature. It is also somewhat less intense than the OSA feature, but the relative intensities of the maxima of the first and second features are almost the same for both OSA and OCSA. The low intensity feature at E(rel) ~ 13 eV in the OCSA XAS spectra is not present for the OSA XAS. Detailed assignments of the character of the OSA and OCSA features for isolated neptunyl are given in Ref. 8. However, the overall conclusion is that if the primary concern is for the effect of hydration on the two most intense features of the XAS, it should be satisfactory to use the OSA spectra to identify the origin of the changes when the isolated molecule is embedded with $NpO_2[H_2O]_5^{2+}$.

III. CONSEQUENCES OF THE HYDRATED ENVIRONMENT FOR THE NEPTUNYL XAS

The consequences of the environment of NpO_2^{2+} in solution leading to changes in the $M_5 \rightarrow 5f$ neptunyl XAS are examined, and the importance of taking the environment into account is established. In Sec. III A, an overview of the differences between isolated and hydrated NpO_2^{2+} is made as a function of the distance between Np and the H_2O molecules, R(Np–H_2O), in $NpO_2[H_2O]_5^{2+}$. In Sec. III B, the orbital and WF properties as a function of R(Np–H_2O) are examined to identify the origin of these changes; in particular, the distinction of purely electrostatic effects of this distance change is contrasted with changes in the electronic structure. We recall that all results in Secs. III A and III B are for the OSA WFs of the excited states.

A. Overview of hydrated NpO_2^{2+}

A comparison between the $M_5 \rightarrow 5f$ XAS obtained using isolated NpO_2^{2+}, shown as a red curve, and hydrated $NpO_2[H_2O]^{2+}$,

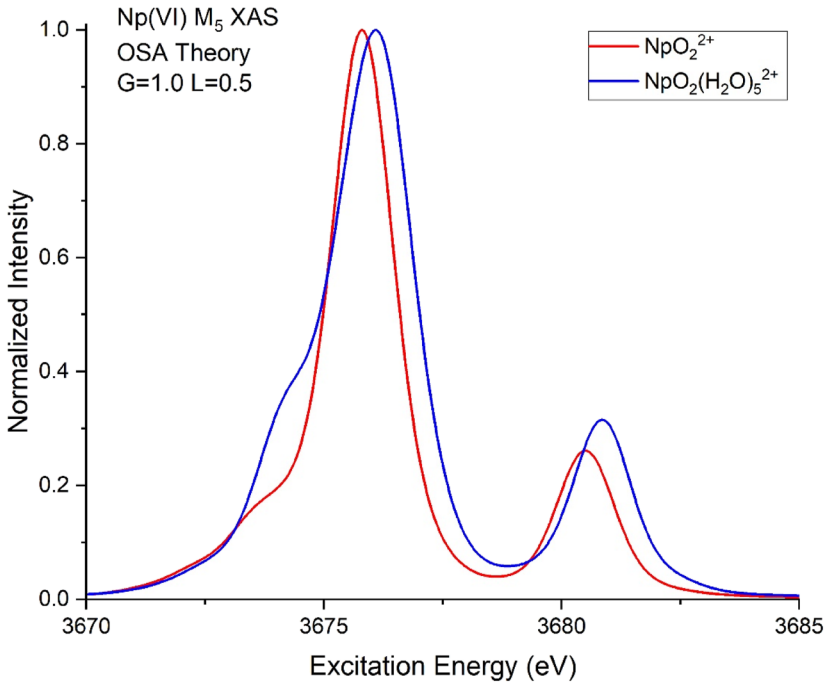

FIG. 7. Comparison of the XAS between isolated (red curve) and hydrated (blue curve) neptunyl obtained with the OSA active space for the excited states; see the text for further details.

shown as a blue curve, is made in Fig. 7. The Np–O and R(Np–H_2O) distances are 1.73 and 2.48 Å, respectively; see Sec. II A; the Voigt broadening parameters are also described in Sec. II A. The transition energies in Fig. 7 are the calculated transition energies rather than the E(rel) used in Figs. 5 and 6. Both plots are made with the OSA level of theory for the excited states to allow a direct comparison between the model of isolated neptunyl and the more realistic hydrated model. The spectra of the two neptunyl models, isolated and hydrated, in Fig. 7 are reasonably similar with two differences. The first concerns the main peak, which is centered at ~3676 eV. This feature is somewhat broader for the hydrated than for the isolated NpO_2^{2+}. In fact, the broader feature for the hydrated NpO_2^{2+} improves the agreement of the theory with the measured XAS; see the isolated NpO_2^{2+} XAS compared to measurement in Fig. 2. There

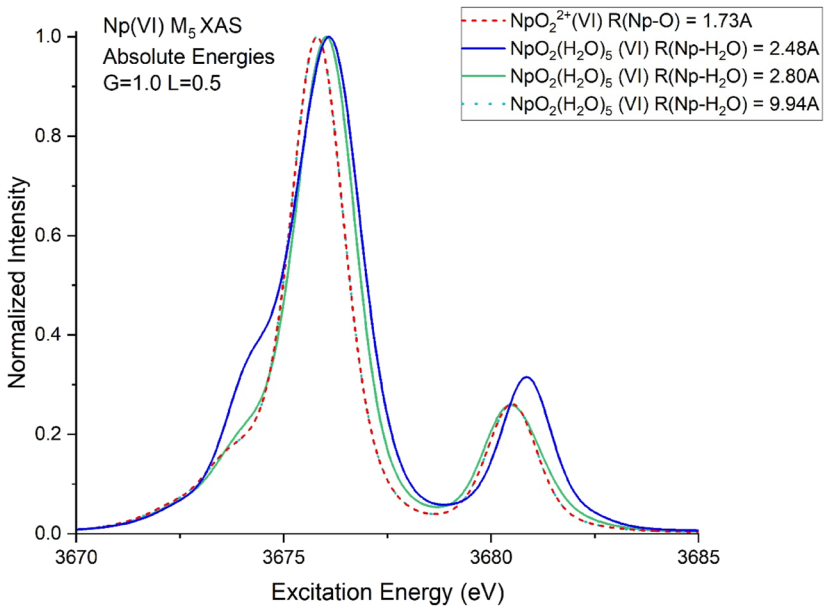

FIG. 8. Comparison of the XAS for four models of NpO_2^{2+}, which includes isolated and three hydrated neptunyls with different distances, R(Np–H_2O). The plots parallel those in Fig. 7.

is relatively little shift between the maxima of the two peaks, indicating that adding the water environment makes only a small change in the energetic difference of the initial and excited states. However, the theoretical transition energy for this first feature is slightly larger than the measured excitation energy by ~5 eV; however, given the very large excitation energies, the error in the transition energy is only 0.1%. The energy of the feature at ~3681 eV is separated from the main peak by ~1 eV more for the hydrated, $NpO_2[H_2O]_5^{2+}$, model of neptunyl compared to the isolated compound. Indeed, the increase in this separation with the hydrated model improves the agreement between theory and experiment; see Fig. 2. In order to better understand the origin of these changes between hydrated and isolated neptunyl, the properties of the hydrated model are examined as a function of the distance between the H_2O and the Np center, R(Np–H_2O).

In Fig. 8, the comparison between the $M_5 \rightarrow$ 5f XAS for isolated and hydrated neptunyl is extended to include two additional distances of R(Np–H_2O) = 2.80 Å, green curve, and R(Np–H_2O) = 9.94 Å, green dashed curve, as well as R(Np–H_2O) = 2.48 Å, blue curve. Also shown in Fig. 8 is the OSA XAS for isolated neptunyl as the red dashed curve. However, as distinct from Fig. 7, we use absolute intensities, see Eq. (1), rather than scaled intensities, in order to better identify the distance dependence of XAS features. It is immediately clear that the $NpO_2[H_2O]_5^{2+}$ XAS curve for R(Np–H_2O) = 9.94 Å is virtually identical to the XAS curve for isolated NpO_2^{2+}; indeed, it is very difficult to distinguish the two curves. This is not at all surprising since at this large R(Np–H_2O), there is essentially no overlap of the H_2O and NpO_2^{2+} charge distributions and the H_2O potential is small and almost constant in the region of the neptunyl charge distribution. It is also important that the relative intensity of the main peak and the feature at ~3681 eV does depend strongly on the R(Np–H_2O) distance.

B. Orbital and wavefunction properties

This section begins with an analysis of the open shell orbital energies of the hydrated cluster, $NpO_2[H_2O]_5^{2+}$, for different R(Np–H_2O) distances; these orbitals are dominantly Np 5f orbitals. It is expected that the interaction energy between NpO_2^{2+} and the water molecules is dominated by electrostatic contributions between the +2 charge of neptunyl and the dipole moment of the five H_2O molecules. If we make the reasonable assumptions that the effective charge of the open shell neptunyl, 5f, orbitals is centered at the Np cation and that the dipole moment of H_2O is centered at the O nucleus, then this electrostatic interaction is proportional to $1/R^2$. The charge–dipole interaction is significantly larger than the next term, proportional to $1/R^3$, arising from the NpO_2^{2+} charge with the H_2O quadrupole. Clearly, this dependence of the electrostatic contribution should apply to orbital energies as well as total energies. Thus, to distinguish the electrostatic interaction from contributions due to changes in the covalent character of neptunyl, the plot in Fig. 9 is made for the 5f orbital energy, ε(5f), with respect to $1/R^2$, which should be linear if the interaction is purely electrostatic. This plot is for the seven DHF 5f orbital energies of the initial GS state $5f^1$ configuration at the R(Np–H_2O) distances shown in Fig. 8 and one additional distance R(Np–H_2O) = 3.1 Å; the orbital energies are in eV, and the distances are in $(Å)^{-2}$. The data for $1/R^2 = 0$ are for isolated NpO_2^{2+}. The seven distinct ε values are labeled according

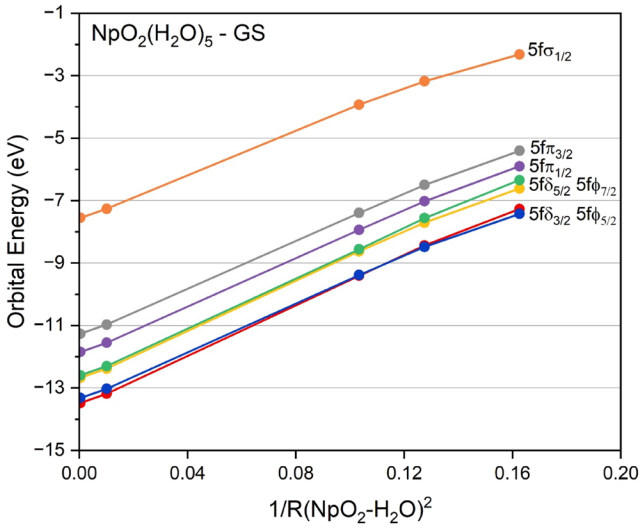

FIG. 9. Plot of the open shell, dominantly Np(5f), orbital energies for the initial state configuration of hydrated NpO_2^{2+} as a function of $1/R(Np–H_2O)^2$ with ε in eV and R in Å; see the text.

to the order of their values for the isolated NpO_2^{2+}; see Eq. (3). As noted previously,[7] the orbitals of NpO_2^{2+} are either non-bonding or anti-bonding between the Np cation and the O anions, and the open shell orbitals for the hydrated cluster, $NpO_2[H_2O]_5^{2+}$, are perturbed orbitals of the isolated cation.

If the interaction between neptunyl and the embedding H_2O molecules were entirely electrostatic, the plots of the ε would be linear in $1/R^2$. It can be observed from Fig. 9 that the behavior of the curves of $\varepsilon(5f_\lambda)$ for all the orbitals is essentially linear with very similar slopes for the different $5f_\lambda$; this is strong evidence that the interaction is essentially electrostatic. Of course, there is significant anti-bonding Np–O covalent character in these orbitals.[7] However, what is required for the orbital energy curves to be linear with respect to the embedding distance is that the covalent character be essentially constant for the different embedding distances. Indeed, this is what should be expected if the role of the embedding H_2O molecules on the neptunyl is purely electrostatic. However, the curves have some departure from linear behavior especially for the largest value of $1/R^2$ or the smallest distance of R(Np–H_2O) = 2.48 Å. While the results in Fig. 9 are for the initial state open shell ε before the excitation of a $3d_{5/2}$ electron into the 5f shell, the properties of the valence open shell ε for the excited configuration, with the $M_5 \rightarrow$ 5f occupations of Eq. (2), are more relevant. The valence open shell ε energies are plotted in Fig. 10 with the same conventions as used in Fig. 9. The differences between the curves in Figs. 9 and 10 are very minor. Mainly, there are almost rigid shifts for the ε(5f) of the excited configuration with respect to those of the initial GS configuration. This guarantees that the conclusions about the dominantly electrostatic role of the embedding H_2O molecules made for the orbitals of the initial state configuration are also relevant for the orbitals of the excited configuration.

Further evidence for the electrostatic role of the water molecules with the hydrated $NpO_2[H_2O]_5^{2+}$ model can be obtained

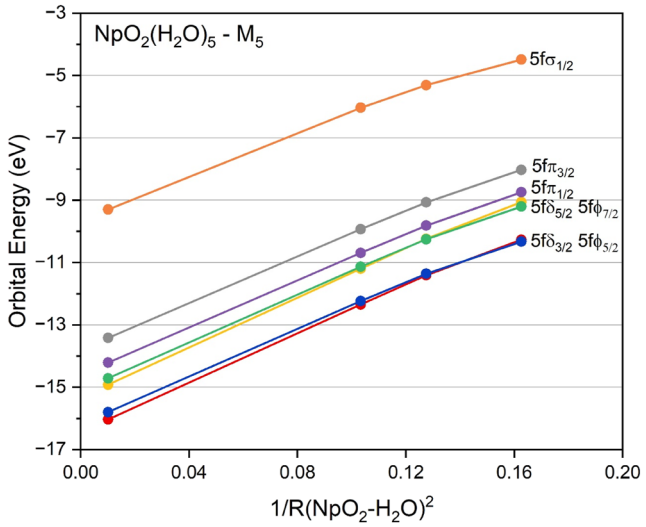

FIG. 10. Plot of the open shell, dominantly Np(5f), orbital energies for the excited $M_5 \rightarrow 5f$ configuration of hydrated NpO_2^{2+} as a function of $1/R(Np–H_2O)^2$ with ε in eV and R in Å; see the text and caption of Fig. 9.

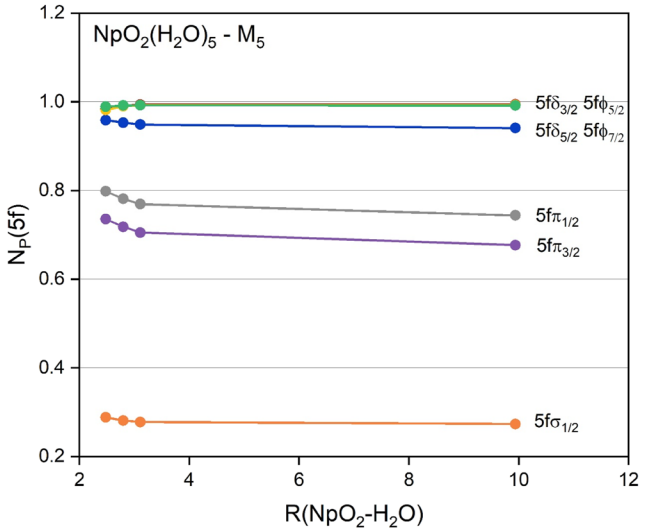

FIG. 11. Plot of the projections of the 5f orbitals of isolated Np(+6) on the valence open shell, dominantly Np(5f), orbitals of optimized for the excited $M_5 \rightarrow 5f$ configuration of hydrated NpO_2^{2+} as a function of $R(NpO_2–H_2O)$; the orbitals of $NpO_2[H_2O]_5^{2+}$ are labeled as in Fig. 10.

from the projection of the 5f orbitals of the Np(+6) cation on the orbitals of the hydrated model as discussed in Sec. II B. The projections of the Np 5f orbitals on the valence open shell orbitals for the excited state, $M_5 \rightarrow 5f$, configuration of the hydrated model, $NpO_2[H_2O]_5^{2+}$, as a function of $R(NpO_2–H_2O)$ are plotted in Fig. 11 for the same distances of R as in Figs. 9 and 10. We do not include the $N_p(5f)$ projections on the orbitals of isolated NpO_2^{2+} since they are essentially identical to the projections of Np(5f) on the open shell orbitals for R = 9.94 Å. The projections are in the same seven sets of orbitals as in Figs. 9 and 10 with the same notation for the orbital sets; however, as discussed below, several of the orbital sets cannot be distinguished in Fig. 11. It is recalled that the orbital projections are in the range $0 \le N_p(5f_\lambda) \le 1$, where the $5f_\lambda$ indicates the projections on each of the seven open shell orbitals. The projections at the largest separation of the H_2O from NpO_2 of R = 9.94 Å and for the next shorter separation of $R(Np–H_2O)$ = 3.40 Å are virtually identical, while for the shorter distances of R = 2.80 and 2.48 Å, there are small changes. The most important conclusion that can be drawn from this near constant behavior of the $N_P(5f)$ with R is that the covalent character of the Np–O interaction remains essentially unchanged by the presence of the embedding H_2O molecules and there is an essentially constant covalent character with respect to $R(Np–H_2O)$. The origin of the small departures from constant projection with R may, in part, be due to a compression of the NpO_2^{2+} orbitals to minimize the Pauli repulsion with the presence of the H_2O charge distribution.[17,40] The curves in Fig. 11 are consistent with the orbital energy curves in Figs. 9 and 10. Furthermore, the nearly constant values of the $N_p(5f)$ in Fig. 11 also give information about the extent of the covalent character of the different open shell orbitals of NpO_2^{2+} as has been discussed earlier for NpO_2^{2+}.[7]

Clearly, the effect of the hydration in the aqueous environment in which the actinyl XAS is actually measured[2] is very minor. As shown above, the covalent character of the open shell, dominantly 5f, orbitals is hardly changed by the presence of the embedding H_2O molecules, even for relatively short distances between the H_2O molecules and the neptunyl cation, NpO_2^{2+}. It is also appropriate to examine the extent to which the total WFs for the excited states change in the presence of the hydrating H_2O. This is done by comparing the properties of the hydrated neptunyl, $NpO_2[H_2O]_5^{2+}$, WFs, for $R(Np–H_2O)$ = 2.48 Å with those of the isolated NpO_2^{2+}; the properties of the WFs for the bare NpO_2^{2+} are shown in Fig. 12(a) and for the hydrated system in Fig. 12(b). These properties are displayed following the methods used earlier to describe the isolated NpO_2^{2+},[8] which are reviewed briefly. The properties considered are the XAS intensity, Eq. (1), and the occupations of the different 5f orbitals in the CI WFs of the excited state multiplet WFs; see Refs. 8 and 41. In order to have a manageable display, the properties are shown for groups of WFs; see Sec. II B. The group intensities are shown in Fig. 12 as yellow vertical bars, and the group average open shell occupations are shown as symbols centered at the group energy. For the shell occupations, the seven ligand and spin–orbit occupations are placed in three sets, the non-bonding ϕ and δ are summed as 5fϕδ, 5fπ for the sum of $\pi_{1/2}$ and $\pi_{3/2}$, and 5fσ. The shell occupations are on the left axis, and the normalized intensities are on the right axis. The group energies are relative to the lowest excitation energy set as E = 0.

There is a strong similarity for the $M_5 \rightarrow 5f$ XAS predicted by isolated and hydrated NpO_2^{2+}; in particular, the characters of the two features observed in the broadened spectra of Fig. 2 are the same in both models. The first feature has occupations mainly of 5fϕδ and 5fπ with the 5fσ contributions being very small. The second feature has occupations mainly of 5fϕδ and 5fσ with only small contributions from 5fπ. The main changes between the two models are that the first intense feature is broader and the splitting of the

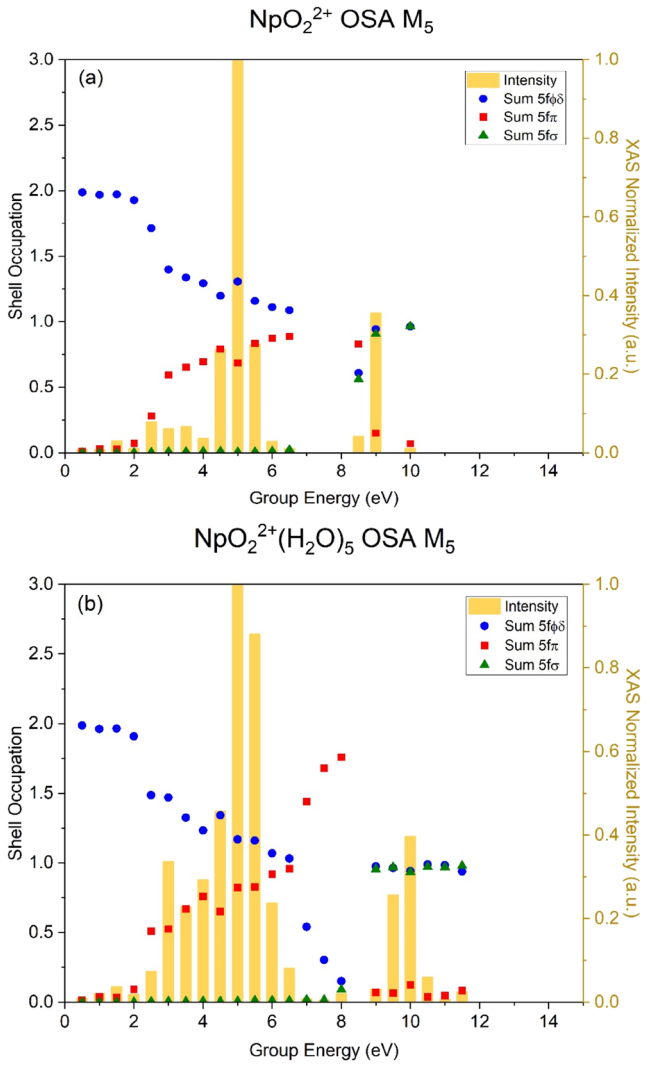

FIG. 12. Properties of the OSA excited state WFs for (a) isolated and (b) hydrated NpO_2^{2+}; see the text for details.

first two features is somewhat larger for the hydrated cluster than for the isolated cluster. This is similar to the differences that are shown in Fig. 7 for the broadened XAS intensities of the two models. The comparison in Fig. 7 shows how the features in the observed XAS arise and depend on the different interactions in the isolated and hydrated models, but it does not give information on the character of the excited states that contribute to the predicted intensity. On the other hand, the information in Fig. 12 does not directly lead to a prediction of the observed XAS intensities since a broadening of the group intensities is not included. However, it does give direct information on the relationship of the 5f occupations of the excited state multiplets to the XAS intensity of these multiplets. In addition, since the occupations are not integral, the many-body character of the excited state multiplets is clearly demonstrated. For a given configuration, the orbital occupation numbers must be integer; non-integral occupations can only be found for CI WFs where different configurations are mixed.

IV. CONCLUSIONS

This paper has established the extent to which a simple model of an isolated neptunium molecule, NpO_2^{2+}, is satisfactory to provide a reliable description of the $M_5 \rightarrow 5f$ excited states and of the XAS spectra of excitations to these states. In particular, this is of concern since the measured XAS spectra have not been for an isolated molecule but for a molecule in solution, and it is necessary to establish the extent to which this environment needs to be taken into account. A model of NpO_2^{2+} that includes the nearest neighbor water molecules was determined to be $NpO_2[H_2O]_5^{2+}$, and the XAS for this model was compared with the XAS for isolated NpO_2^{2+}. However, in order to make this comparison, it was necessary to use a simpler theoretical model where only the open shell orbitals and electrons were included in the active space for the many-body wavefunctions. It was established that this simpler model was adequate to describe the main features of the $M_5 \rightarrow 5f$ XAS with reasonable accuracy. In addition, the importance of the hydration on the XAS was investigated by studying the properties of the excited $M_5 \rightarrow 5f$ multiplets as a function of the distance of the embedding H_2O molecules in the $NpO_2[H_2O]_5^{2+}$ cluster from NpO_2^{2+}. These investigations of the excited multiplets involved analyses of both the open shell orbital character and the wavefunction character. For the orbital character, the orbital energies and the projections of the Np 5f composition of the open shell orbitals were examined with the conclusion that changes in the character of the orbitals, especially their covalency, were not affected significantly by the presence of the embedding H_2O molecules. For the wavefunction character, the orbital composition of the excited multiplets and the distribution of the XAS intensity with respect to the excitation energies of the excited multiplets were shown to be perturbed only slightly by the presence of the embedding H_2O molecules. Overall, these theoretical tests give compelling evidence that the main XAS features can be reliably described with a model of an isolated NpO_2^{2+} cation. It is expected that this conclusion also holds for other actinyls.

ACKNOWLEDGMENTS

P.S.B. acknowledges the support from the U.S. Department of Energy, Office of Science, Office of Basic Energy Sciences, Chemical Sciences, Geosciences, and Biosciences (CSGB) Division through its Geosciences program at Pacific Northwest National Laboratory (PNNL). PNNL is a multi-program national laboratory operated for the DOE by the Battelle Memorial Institute under Contract No. DE-AC05-76RL01830. B.S. and T.V. acknowledge funding from the European Research Council (ERC) Consolidator Grant 2020 under the European Union's Horizon 2020 research and innovation program (Grant Agreement No. 101003292).

AUTHOR DECLARATIONS

Conflict of Interest

The authors have no conflicts to disclose.

Author Contributions

Paul S. Bagus: Conceptualization (equal); Formal analysis (equal); Funding acquisition (equal); Methodology (equal); Validation (equal); Visualization (equal); Writing – original draft (lead). **Connie J. Nelin**: Conceptualization (equal); Formal analysis (equal); Investigation (equal); Methodology (equal); Visualization (lead); Writing – original draft (lead). **Michael Trumm**: Visualization (supporting). **Bianca Schacherl**: Conceptualization (equal); Data curation (equal); Investigation (equal); Writing – review & editing (equal). **Tonya Vitova**: Conceptualization (equal); Data curation (equal); Investigation (equal); Writing – review & editing (equal).

DATA AVAILABILITY

The data that support the findings of this study are available within the article and its references.

REFERENCES

[1] R. G. Denning, "Electronic structure and bonding in actinyl ions and their analogs," J. Phys. Chem. A **111**, 4125–4143 (2007).

[2] T. Vitova, I. Pidchenko, D. Fellhauer, P. S. Bagus, Y. Joly, T. Pruessmann, S. Bahl, E. Gonzalez-Robles, J. Rothe, M. Altmaier, M. A. Denecke, and H. Geckeis, "The role of the 5*f* valence orbitals of early actinides in chemical bonding," Nat. Commun. **8**, 16053 (2017).

[3] F. Gendron, D. Páez-Hernández, F.-P. Notter, B. Pritchard, H. Bolvin, and J. Autschbach, "Magnetic properties and electronic structure of neptunyl(VI) complexes: Wavefunctions, orbitals, and crystal-field models," Chem. - Eur. J. **20**, 7994–8011 (2014).

[4] D.-C. Sergentu, T. J. Duignan, and J. Autschbach, "Ab initio study of covalency in the ground versus core-excited states and X-ray absorption spectra of actinide complexes," J. Phys. Chem. Lett. **9**, 5583–5591 (2018).

[5] R. Polly, B. Schacherl, J. Rothe, and T. Vitova, "Relativistic multiconfigurational *ab initio* calculation of uranyl 3d4f resonant inelastic X-ray scattering," Inorg. Chem. **60**, 18764–18776 (2021).

[6] K. Stanistreet-Welsh and A. Kerridge, "Bounding $[AnO_2]^{2+}$ (An = U, Np) covalency by simulated O K-edge and an M-edge X-ray absorption near-edge spectroscopy," Phys. Chem. Chem. Phys. **25**, 23753 (2023).

[7] P. S. Bagus, C. J. Nelin, K. M. Rosso, B. Schacherl, and T. Vitova, "Electronic structure of actinyls: Orbital properties," Inorg. Chem. **63**, 1793 (2024).

[8] P. S. Bagus, C. J. Nelin, B. Schacherl, and T. Vitova, "Actinyl electronic structure probed by XAS: The role of many-body effects," Inorg. Chem. **63**, 13202 (2024).

[9] T. Saue, R. Bast, A. S. P. Gomes, H. J. A. Jensen, L. Visscher, I. A. Aucar, R. Di Remigio, K. G. Dyall, E. Eliav, E. Fasshauer, T. Fleig, L. Halbert, E. D. Hedegård, B. Helmich-Paris, M. Iliaš, C. R. Jacob, S. Knecht, J. K. Laerdahl, M. L. Vidal, M. K. Nayak, M. Olejniczak, J. M. H. Olsen, M. Pernpointner, B. Senjean, A. Shee, A. Sunaga, and J. N. P. van Stralen, "The DIRAC code for relativistic molecular calculations," J. Chem. Phys. **152**, 204104 (2020).

[10] G. Burns, *Introduction to Group Theory with Applications* (Academic Press, New York, 1977).

[11] H. A. Bethe and E. W. Salpeter, *Quantum Mechanics of One- and Two-Electron Atoms* (Academic Press, 1957).

[12] P. O. Löwdin, "Quantum theory of many-particle systems. I. Physical interpertations by means of density matrices, natural spin-orbitals, and convergence problems in the method of configurational interaction," Phys. Rev. **97**, 1474–1489 (1955).

[13] T. Vitova, I. Pidchenko, D. Fellhauer, T. Pruessmann, S. Bahl, K. Dardenne, T. Yokosawa, B. Schimmelpfennig, M. Altmaier, M. Denecke, J. Rothe, and H. Geckeis, "Exploring the electronic structure and speciation of aqueous and colloidal Pu with high energy resolution XANES and computations," Chem. Commun. **54**, 12824–12827 (2018).

[14] J. Rothe, M. Altmaier, R. Dagan, K. Dardenne, D. Fellhauer, X. Gaona, E. González-Robles Corrales, M. Herm, K. O. Kvashnina, V. Metz, I. Pidchenko, D. Schild, T. Vitova, and H. Geckeis, "Fifteen years of radionuclide research at the KIT synchrotron source in the context of the nuclear waste disposal safety case," Geosciences **9**, 91 (2019).

[15] J. Rothe, S. Butorin, K. Dardenne, M. A. Denecke, B. Kienzler, M. Löble, V. Metz, A. Seibert, M. Steppert, T. Vitova, C. Walther, and H. Geckeis, "The INE-Beamline for actinide science at ANKA," Rev. Sci. Instrum. **83**, 043105 (2012).

[16] T. Vitova, I. Pidchenko, D. Schild, T. Prüßmann, V. Montoya, D. Fellhauer, X. Gaona, E. Bohnert, J. Rothe, R. J. Baker, and H. Geckeis, "Competitive reaction of neptunium(V) and uranium(VI) in potassium–sodium carbonate-rich aqueous media: Speciation study with a focus on high-resolution X-ray spectroscopy," Inorg. Chem. **59**, 8–22 (2020).

[17] I. N. Levine, *Quantum Chemistry* (Prentice-Hall, Upper Saddle River, NJ, 2000).

[18] J. C. Slater, *Quantum Theory of Atomic Structure* (McGraw-Hill, New York, 1960), Vol. 1–2.

[19] A. Ikeda-Ohno, C. Hennig, A. Rossberg, H. Funke, A. C. Scheinost, G. Bernhard, and T. Yaita, "Electrochemical and complexation behavior of neptunium in aqueous perchlorate and nitrate solutions," Inorg. Chem. **47**, 8294–8305 (2008).

[20] R. Antonio, L. Soderholm, C. W. Williams, J.-P. Blaudeau, and B. E. Bursten, "Neptunium redox speciation," Radiochim. Acta **89**, 17–26 (2001).

[21] A. D. Becke, "A new mixing of Hartree–Fock and local density-functional theories," J. Chem. Phys. **98**, 1372–1377 (1993).

[22] C. Lee, W. Yang, and R. G. Parr, "Development of the Colle-Salvetti correlation-energy formula into a functional of the electron density," Phys. Rev. B **37**, 785–789 (1988).

[23] G. Herzberg, *Electronic Spectra and Electronic Structure of Polyatomic Molecules* (Van Nostrand Reinhold, New York, 1966).

[24] G. Herzberg, *Molecular Spectra and Molecular Structure* (Van Nostrand, Princeton, 1950), Vol. 1.

[25] L. Visscher, O. Visser, P. J. C. Aerts, H. Merenga, and W. C. Nieuwpoort, "Relativistic quantum chemistry: The MOLFDIR program package," Comput. Phys. Commun. **81**, 120–144 (1994).

[26] D. Briggs and M. P. Seah, *Practical Surface Analysis* (Wiley, 1983), Vol. 1.

[27] J. L. Campbell and T. Papp, "Widths of the atomic *K*–*N7* levels," At. Data Nucl. Data Tables **77**, 1–56 (2001).

[28] J. A. Gubner, "A new series for approximating Voigt functions," J. Phys. A: Math. Gen. **27**, L745–L749 (1994).

[29] P. S. Bagus, C. J. Nelin, B. Schacherl, T. Vitova, and R. Polly, "Bonding and interactions in UO_2^{2+} for ground and core excited states: Extracting chemistry from molecular orbital calculations," J. Phys. Chem. A **128**, 8024 (2024).

[30] DIRAC, a relativistic *ab initio* electronic structure program, release DIRAC14 (2014), written by T. Saue, L. Visscher, H. J. A. Jensen, and R. Bast with contributions from V. Bakken, K. G. Dyall, S. Dubillard, U. Ekström, E. Eliav, T. Enevoldsen, E. Faßhauer, T. Fleig, O. Fossgaard, A. S. P. Gomes, T. Helgaker, J. Henriksson, M. Iliaš, C. R. Jacob, S. Knecht, S. Komorovský, O. Kullie, C. V. Larsen, J. K. Lærdahl, Y. S. Lee, H. S. Nataraj, P. Norman, G. Olejniczak, J. Olsen, Y. C. Park, J. K. Pedersen, M. Pernpointner, R. di Remigio, K. Ruud, P. Sałek, B. Schimmelpfennig, J. Sikkema, A. J. Thorvaldsen, J. Thyssen, J. van Stralen, S. Villaume, O. Visser, T. Winther, and S. Yamamoto, see http://www.diracprogram.org.

[31] K. G. Dyall, "Relativistic double-zeta, triple-zeta, and quadruple-zeta basis sets for the actinides Ac–Lr," Theor. Chem. Acc. **117**, 491–500 (2007).

[32] F. B. Duijneveldt, "Gaussian basis sets for the atoms He-Ne for use in molecular calculations," Technical Report No. IBM RJ945, 1971.

[33] CLIPS is a program system to compute *ab initio* SCF and correlated wavefunctions for polyatomic systems. It has been developed based on the publicly available programs in the ALCHEMY package from the IBM San Jose Research Laboratory by P. S. Bagus, B. Liu, A. D. McLean, and M. Yoshimine.

[34] R. S. Mulliken, "Electronic population analysis on LCAO-MO molecular wave functions. III. Effects of hybridization on overlap and gross AO populations," J. Chem. Phys. **23**, 2338–2342 (1955).

[35] R. S. Mulliken, "Electronic population analysis on LCAO-MO molecular wave functions. IV. Bonding and antibonding in LCAO and valence-bond theories," J. Chem. Phys. **23**, 2343–2346 (1955).

[36]R. S. Mulliken, "Electronic population analysis on LCAO–MO molecular wave functions. I," J. Chem. Phys. **23**, 1833–1840 (1955).
[37]R. S. Mulliken, "Electronic population analysis on LCAO–MO molecular wave functions. II. Overlap populations, bond orders, and covalent bond energies," J. Chem. Phys. **23**, 1841–1846 (1955).
[38]P. S. Bagus, C. J. Nelin, D. A. Hrovat, and E. S. Ilton, "Covalent bonding in heavy metal oxides," J. Chem. Phys. **146**, 134706 (2017).
[39]J. P. Desclaux, "Relativistic Dirac-Fock expectation values for atoms with $Z = 1$ to $Z = 120$," At. Data Nucl. Data Tables **12**, 311–406 (1974).
[40]P. S. Bagus, C. R. Brundle, and B. V. Crist, "Shake loss intensities in x-ray photoelectron spectroscopy: Theory, experiment, and atomic composition accuracy for MgO and related compounds," J. Vac. Sci. Technol. A **39**, 063206 (2021).
[41]L. D. Landau and E. M. Lifshitz, *Quantum Mechanics* (Addison-Wesley, Reading, 1958).